Interharmonic Analysis Model of Photovoltaic Grid-connected System with Extended Dynamic Phasors

Qing Zhong, Yangxin Qiu, Yuming Zhao, Haifeng Li, Gang Wang, and Fushuan Wen

***Abstract*—The interactions between randomly fluctuating power outputs from photovoltaic (PV) at the DC side and background voltage distortions at the AC side could generate interharmonics in the PV grid-connected system (PVGS). There is no universal method that can reveal the transmission mechanism of interharmonics and realize accurate calculation in different scenarios where interharmonics exist in the PVGS. Therefore, extended dynamic phasors (EDPs) and EDP sequence components (EDPSCs) are employed in the interharmonic analysis of the PVGS. First, the dynamic phasors (DPs) and dynamic phasor sequence components (DPSCs) are extended into EDPs and EDPSCs by selecting a suitable fundamental frequency other than the power frequency. Second, an interharmonic analysis model of the PVGS is formulated as a set of state space equations. Third, with the decoupling characteristics of EDPSCs, generation principles and interactions among the interharmonics in the PVGS are presented by the sequence components, and its correctness is verified by simulation and experiment. The presented model can be used to accurately calculate the interharmonics generated in the PVGS both at the AC and DC sides. Because of the decoupling among the EDPSCs, the set of state space equations can effectively describe the principle.**

***Index Terms*—Dynamic phasor sequence component (DPSC), harmonic, interharmonic, photovoltaic grid-connected system (PVGS), power quality.**

I. Introduction

In recent years, photovoltaic (PV) generation has been gradually changing the morphology and structure of power systems by interconnecting with the concerned distribution network [1], [2]. However, PV generation could result in power quality problems in the distribution system because nonlinear power electronic converters are used as grid-connected interfaces. The interharmonic is one of the most significant power quality problems in PV grid-connected systems (PVGSs), and has been attracting increasing attentions [3]-[5]. When a large interharmonic current is injected into the power system, some problems such as voltage fluctuations and flicker, metering errors, relay malfunctions, and motor vibration threaten the normal operation of the power system [6], [7]. The interharmonics can also induce subsynchronous oscillations in the power system, endangering the security and stability of the power system [8]. With the increasing penetration of PV generation in the power system and the interactions among the inverters, the interharmonic problem in the PVGS has become increasingly complicated. Therefore, it is necessary to develop a generally applicable analysis model for the PVGS as a theoretical analysis tool for mitigating the interharmonics.

To date, some research works have been conducted on the harmonics generated by distributed PV generation. A frequency domain model is presented to study the harmonic in a large PV station in [9], which demonstrates that high-order harmonics produced by the PV station are almost close to the switch frequency. The output harmonic currents are significantly affected by the light and temperature conditions. The simulation results in [10] show that the total harmonic distortion (THD) decreases significantly when the level number of the modular multi-level converter (MMC) in the PVGS increases. A state-space model is established in [11] to analyze the harmonic interactions between the AC and DC sides as well as the harmonic inability of the PVGS. The studies of integer harmonics in the PVGS are relatively complete. However, the studies of interharmonics are rare.

Interharmonics whose frequency is non-integer multiples of the power frequency are usually caused by mutual modulation between different frequency systems. Many existing research works address interharmonics in speed regulation systems, high-voltage direct current (HVDC) transmission systems, wind power plants, and induction motors [12]-[15]. The experimental results in [16] show that a PV inverter connected to a weak power grid can generate more interharmonic currents, especially when the parameters of the phase-locked loop (PLL) are not properly specified. Interharmonic analysis models are proposed in [17], [18] with the characteristics of interharmonics caused by maximum power point tracking (MPPT) modulation. The impact of the background

Manuscript received: April 17, 2020; accepted: September 14, 2020. Date of CrossCheck: September 14, 2020. Date of online publication: June 25, 2021.

This work was supported by China Southern Power Grid Co., Ltd. (No. 090000KK52180116).

This article is distributed under the terms of the Creative Commons Attribution 4.0 International License (http://creativecommons.org/licenses/by/4.0/).

Q. Zhong, Y. Qiu (corresponding author), H. Li, and G. Wang are with the School of Electric Power, South China University of Technology, Guangzhou, China (e-mail: epqzhong@scut.edu.cn; 915135943@qq.com; lihf@scut.edu.cn; wanggang@scut.edu.cn).

Y. Zhao is with Shenzhen Power Supply Bureau Co., Ltd., Shenzhen, China (e-mail: zhaoym98@sina.com).

F. Wen is with the School of Electrical Engineering, Zhejiang University, Hangzhou, China (e-mail: fushuan.wen@gmail.com).

DOI: 10.35833/MPCE.2020.000241

voltage distortion on the interharmonics of the PV inverter is investigated in [19], and is dependent on the PV inverter topologies, control strategies, and the design of the PLL. The literature on interharmonics has focused on qualitative analysis rather than quantitative calculation. In [20], a qualitative calculation method for the interharmonics of converters is proposed. However, it only considers the influence of the PLL instead of the switching functions. Random power fluctuations of the PV at the DC side and background voltage distortions at the AC side are the two main sources for generating interharmonics. However, it is very difficult to explain the interharmonic interactions between the PV and power grid. A generic mathematical model is still not available for describing the interharmonics in the PVGS, especially when there are interharmonic sources at both the AC and DC sides, which will be addressed in this paper.

A well-established dynamic phasor (DP), which is widely employed in analyzing harmonic interactions among converters, can be employed to analyze the interharmonic problem in the PVGS [21]. However, most of the existing research works on DP-based interharmonics only consider the harmonic whose frequency is integer multiples of the power frequency [22], [23]. In defining the unbalance for interharmonics, the phase sequence of positive-order DPs is considered [24]. However, the negative-order DPs are not included but are essential when there are multiplicative terms in the mathematical model.

With the above background, an extended DP (EDP) and EDP sequence components (EDPSCs) are employed to establish the analysis model of the PVGS. First, a method to extend the granularity of the DPs and DP sequence components (DPSCs) is presented. The granularity can be properly selected to satisfy the demand of interharmonic analysis. Second, the EDPSCs of the current at the AC side and the EDPs of the voltage at the DC side are selected as the state variables. The EDPSCs of the PV output current at the DC side and the EDPs of the source voltage at the AC side are selected as the input/control variables. The interharmonic analysis model of the PVSG is formulated as state space equations. Third, the principles of generating the interactions among interharmonics in the PVSG can be deduced from the decoupling characteristics of the EDPSCs. Finally, simulations and experiments are performed to verify the correctness of the presented model.

The remainder of this paper is organized as follows. Section II introduces the basics of the DPs and DPSCs. The method of attaining the EDPs and EDPSCs as well as their characteristics are presented with granularity extension. Section III presents the analysis model of the PVSG as a set of state-space equations, the principles of generation and interactions among interharmonics in PVSG are analyzed. The simulation model and experimental platform are presented in Section IV, and the simulation and experimental results are compared to demonstrate the correctness of the presented analysis model. The paper is concluded in Section V.

II. Extension of DPs and DPSCs

The DP is proposed based on time-varying Fourier decomposition. The signal $x(t)$ in the time domain can be expressed as a Fourier series in time interval $\left(t-T_s, t\right]$, where T_s is the period of $x(t)$ and $x\left(t-T_s\right)=x(t)$, as shown in (1).

$$x(t)=\sum_{k=-\infty}^{+\infty}\langle X\rangle_k \mathrm{e}^{\mathrm{j}k\omega_s t} \tag{1}$$

where ω_s is the fundamental angular frequency, which is selected as the power angular frequency, and $\omega_s T_s=2\pi$; and $\langle X\rangle_k$ is the k^{th} DP of $x(t)$, as shown in (2).

$$\langle X\rangle_k=\frac{1}{T_s}\int_{t-T_s}^{t} x(\tau)\mathrm{e}^{-\mathrm{j}k\omega_s\tau}\mathrm{d}\tau \tag{2}$$

For a three-phase system, DPs can be transformed into DPSCs by symmetrical transformation, as shown in (3).

$$\begin{bmatrix}\langle X_{a(1)}\rangle_k\\ \langle X_{a(2)}\rangle_k\\ \langle X_{a(0)}\rangle_k\end{bmatrix}=\boldsymbol{T}\begin{bmatrix}\langle X_a\rangle_k\\ \langle X_b\rangle_k\\ \langle X_c\rangle_k\end{bmatrix} \tag{3}$$

$$\boldsymbol{T}=\frac{1}{3}\begin{bmatrix}1 & \mathrm{e}^{\mathrm{j}120^\circ} & \mathrm{e}^{-\mathrm{j}120^\circ}\\ 1 & \mathrm{e}^{-\mathrm{j}120^\circ} & \mathrm{e}^{\mathrm{j}120^\circ}\\ 1 & 1 & 1\end{bmatrix} \tag{4}$$

where $\langle X_{a(1)}\rangle_k$, $\langle X_{a(2)}\rangle_k$, and $\langle X_{a(0)}\rangle_k$ are the positive-, negative-, and zero-sequence components of the k^{th} DP, respectively; and $\langle X_a\rangle_k$, $\langle X_b\rangle_k$, and $\langle X_c\rangle_k$ are the k^{th} DPs of phase a, phase b, and phase c, respectively. The DPSCs has "derivative", "convolution", "conjugate" and other characteristics [21].

Since the interharmonics' frequency is non-integer multiples of the power frequency, the traditional DP is not suitable for the analysis of interharmonincs. The granularity must be extended. Therefore, by selecting ω as the fundamental angular frequency, the DP can be extended as:

$$\langle X\rangle_k^E=\frac{1}{T}\int_{t-T}^{t} x(\tau)\mathrm{e}^{-\mathrm{j}k\omega\tau}\mathrm{d}\tau \tag{5}$$

where $\langle X\rangle_k^E$ is the k^{th} EDP, which can also be treated as the interharmonic of the system, and $T=2\pi/\omega$. To analyze both the interharmonics and harmonics, the selected fundamental angular frequency should meet the requirements for the frequency resolution of measuring the interharmonics in standards. The power angular frequency has to be an integer multiple of the selected fundamental angular frequency, as $\omega_s=m\omega$, where m is a positive integer. For example, the standards for interharmonics specify 5 Hz as the frequency resolution for measuring interharmonics [25]. Thus, the selected fundamental frequency for the EDP should be selected as 5 Hz.

With the symmetrical transformation, the three-phase EDPs can be transformed into sequence components as:

$$\begin{bmatrix}\langle X_{a(1)}\rangle_k^E\\ \langle X_{a(2)}\rangle_k^E\\ \langle X_{a(0)}\rangle_k^E\end{bmatrix}=\boldsymbol{T}\begin{bmatrix}\langle X_a\rangle_k^E\\ \langle X_b\rangle_k^E\\ \langle X_c\rangle_k^E\end{bmatrix} \tag{6}$$

where $\langle X_{a(1)}\rangle_k^E$, $\langle X_{a(2)}\rangle_k^E$, and $\langle X_{a(0)}\rangle_k^E$ are the positive-, negative-, and zero-sequence components of the k^{th} EDPs, respectively, which are referred to as EDPSCs; and $\langle X_a\rangle_k^E$, $\langle X_b\rangle_k^E$, and $\langle X_c\rangle_k^E$ are the k^{th} EDPs of phase a, phase b, and phase c, respectively. The EDPSCs have the same characteristics as the DPSCs, which can realize the decoupling of the sequence components.

III. Interharmonic Analysis Model of PVGS

A. Time Domain Model of PVGS

A single-stage grid-connected PV inverter is used as the research object, as shown in Fig. 1, and U_{sa}, U_{sb}, and U_{sc} are the source voltages; U_{ca}, U_{cb}, and U_{cc} are the output voltages of phase a, phase b, and phase c at the AC side, respectively; U_{dc} is the voltage at the DC side; I_a, I_b, and I_c are the output currents of phase a, phase b, and phase c at the AC side, respectively; I_{dc} is the input current at the DC side; I_{pv} is the output current of the PV array; C is the capacitor at the DC side; $U_N=\left(U_{sa}+U_{sb}+U_{sc}\right)/3$ is the voltage of the neutral point; and R and L are the equivalent resistance and inductance of the filter at the AC side, respectively.

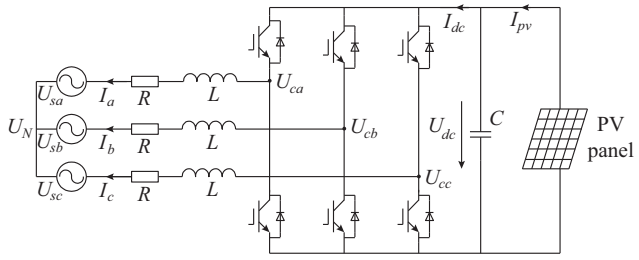

Fig. 1. Diagram of single-stage grid-connected PV inverter.

The model of the PV inverter in the time domain is given as:

$$\begin{cases} L\dfrac{\mathrm{d}I_a}{\mathrm{d}t}=U_{dc}\left(\dfrac{2}{3}S_a-\dfrac{1}{3}S_b-\dfrac{1}{3}S_c\right)-RI_a-\left(U_{sa}-U_N\right) \\ L\dfrac{\mathrm{d}I_b}{\mathrm{d}t}=U_{dc}\left(\dfrac{2}{3}S_b-\dfrac{1}{3}S_c-\dfrac{1}{3}S_a\right)-RI_b-\left(U_{sb}-U_N\right) \\ L\dfrac{\mathrm{d}I_c}{\mathrm{d}t}=U_{dc}\left(\dfrac{2}{3}S_c-\dfrac{1}{3}S_a-\dfrac{1}{3}S_b\right)-RI_c-\left(U_{sc}-U_N\right) \\ C\dfrac{\mathrm{d}U_{dc}}{\mathrm{d}t}=I_{pv}-\left(I_aS_a+I_bS_b+I_cS_c\right) \end{cases} \tag{7}$$

where S_a, S_b, and S_c are the three-phase switching functions representing the switch state of the power electronic devices, which equals 1 if the switch is on, and equals 0 otherwise.

B. Interharmonic Analysis Model of PVGS

Similar to the harmonic analysis model of the VSC based on the DPSCs in [21], the time domain model can be transformed into the equations described by the EDPSCs. The differential equations of the k^{th} EDPSCs of the currents at the AC side and the EDPs of the voltage at the DC side are expressed as:

$$\begin{cases} L\dfrac{\mathrm{d}\langle I_{a(1)}\rangle_k^E}{\mathrm{d}t}=-\left(R+\mathrm{j}k\omega L\right)\langle I_{a(1)}\rangle_k^E-\langle U_{sa(1)}\rangle_k^E+\sum\limits_i\langle S_{a(1)}\rangle_i^E\langle U_{dc}\rangle_{k-i}^E \\ L\dfrac{\mathrm{d}\langle I_{a(2)}\rangle_k^E}{\mathrm{d}t}=-\left(R+\mathrm{j}k\omega L\right)\langle I_{a(2)}\rangle_k^E-\langle U_{sa(2)}\rangle_k^E+\sum\limits_i\langle S_{a(2)}\rangle_i^E\langle U_{dc}\rangle_{k-i}^E \\ C\dfrac{\mathrm{d}\langle U_{dc}\rangle_k^E}{\mathrm{d}t}=-3\left(\sum\limits_i\langle S_{a(2)}\rangle_i^E\langle I_{a(1)}\rangle_{k-i}^E+\sum\limits_i\langle S_{a(1)}\rangle_i^E\langle I_{a(2)}\rangle_{k-i}^E\right)+ \\ \qquad\qquad \langle I_{pv}\rangle_k^E-\mathrm{j}\omega C\langle U_{dc}\rangle_k^E \end{cases} \tag{8}$$

where $\langle I_{a(1)}\rangle_k^E$ and $\langle I_{a(2)}\rangle_k^E$ are the positive- and negative-sequence components of the k^{th} EDPSCs of I_a, respectively; $\langle U_{sa(1)}\rangle_k^E$ and $\langle U_{sa(2)}\rangle_k^E$ are the positive- and negative-sequence components of the k^{th} EDPSCs of U_{sa}, respectively; $\langle S_{a(1)}\rangle_i^E$ and $\langle S_{a(2)}\rangle_i^E$ are the positive- and negative-sequence components of the i^{th} EDPSCs of S_a, respectively; $\langle I_{pv}\rangle_k^E$ is the k^{th} EDPs of I_{pv}; and $\langle U_{dc}\rangle_k^E$ and $\langle U_{dc}\rangle_{k-i}^E$ are the k^{th} and $(k-i)^{\text{th}}$ EDPs of U_{dc}, respectively.

Selecting the analysis scope of interharmonics, which is from 0 to $n-1$ here, the EDPSCs of the current at the AC side and the EDPs of the voltage at the DC side are defined as the state variables $\boldsymbol{X}_1$ and $\boldsymbol{X}_2$, respectively, which are expressed as:

$$\begin{aligned} \boldsymbol{X}_1=\Big[&\langle I_{a(1)}\rangle_0^E,\langle I_{a(2)}\rangle_0^E,\langle I_{a(0)}\rangle_0^E,\langle I_{a(1)}\rangle_1^E,\langle I_{a(2)}\rangle_1^E, \\ &\langle I_{a(0)}\rangle_1^E,\ldots,\langle I_{a(1)}\rangle_{n-1}^E,\langle I_{a(2)}\rangle_{n-1}^E,\langle I_{a(0)}\rangle_{n-1}^E\Big]^{\mathrm{T}} \end{aligned} \tag{9}$$

$$\boldsymbol{X}_2=\left[\langle U_{dc}\rangle_0^E,\langle U_{dc}\rangle_1^E,\ldots,\langle U_{dc}\rangle_{n-1}^E\right]^{\mathrm{T}} \tag{10}$$

The EDPSCs of the source voltage at the AC side and the EDPs of the PV output current at the DC side are defined as the input variables $\boldsymbol{U}_1$ and $\boldsymbol{U}_2$, respectively, which are given as:

$$\begin{cases} \boldsymbol{U}_1=\Big[\langle U_{sa(1)}\rangle_0^E,\langle U_{sa(2)}\rangle_0^E,\langle U_{sa(0)}\rangle_0^E,\langle U_{sa(1)}\rangle,\langle U_{sa(2)}\rangle_1^E, \\ \qquad\langle U_{sa(0)}\rangle_1^E,\ldots,\langle U_{sa(1)}\rangle_{n-1}^E,\langle U_{sa(2)}\rangle_{n-1}^E,\langle U_{sa(0)}\rangle_{n-1}^E\Big]^{\mathrm{T}} \\ \boldsymbol{U}_2=\left[\langle I_{pv}\rangle_0^E,\langle I_{pv}\rangle_1^E,\ldots,\langle I_{pv}\rangle_{n-1}^E\right]^{\mathrm{T}} \end{cases} \tag{11}$$

Equation (8) can then be rewritten as the state space equation, which is expressed as:

$$\begin{bmatrix} \dfrac{\mathrm{d}\boldsymbol{X}_1}{\mathrm{d}t} \\ \dfrac{\mathrm{d}\boldsymbol{X}_2}{\mathrm{d}t} \end{bmatrix}=\begin{bmatrix} \boldsymbol{A}_{11} & \boldsymbol{A}_{12} \\ \boldsymbol{A}_{21} & \boldsymbol{A}_{21} \end{bmatrix}\begin{bmatrix} \boldsymbol{X}_1 \\ \boldsymbol{X}_2 \end{bmatrix}+\begin{bmatrix} -\boldsymbol{U}_1/L \\ \boldsymbol{U}_2/C \end{bmatrix} \tag{12}$$

The coefficient matrices $\boldsymbol{A}_{11}$, $\boldsymbol{A}_{12}$, $\boldsymbol{A}_{21}$, and $\boldsymbol{A}_{22}$ are:

$$\begin{aligned} \boldsymbol{A}_{11}=\mathrm{diag}\big(&-R/L,-R/L,-R/L,-R/L-\mathrm{j}\omega,-R/L-\mathrm{j}\omega, \\ &-R/L-\mathrm{j}\omega,\ldots,-R/L-\mathrm{j}(n-1)\omega\big) \end{aligned} \tag{13}$$

$$\begin{cases} \boldsymbol{A}_{12}=\dfrac{1}{L}\begin{bmatrix} \langle S_{a(1)}\rangle_0^E & \langle S_{a(2)}\rangle_1^{E^*} & \cdots & \langle S_{a(2)}\rangle_{n-2}^{E^*} & \langle S_{a(2)}\rangle_{n-1}^{E^*} \\ \langle S_{a(2)}\rangle_0^E & \langle S_{a(1)}\rangle_1^{E^*} & \cdots & \langle S_{a(1)}\rangle_{n-2}^{E^*} & \langle S_{a(1)}\rangle_{n-1}^{E^*} \\ 0 & 0 & \cdots & 0 & 0 \\ \vdots & \vdots & & \vdots & \vdots \\ \langle S_{a(1)}\rangle_{n-1}^E & \langle S_{a(1)}\rangle_{n-2}^E & \cdots & \langle S_{a(1)}\rangle_1^E & \langle S_{a(1)}\rangle_0^E \\ \langle S_{a(2)}\rangle_{n-1}^E & \langle S_{a(2)}\rangle_{n-2}^E & \cdots & \langle S_{a(2)}\rangle_1^E & \langle S_{a(2)}\rangle_0^E \\ 0 & 0 & \cdots & 0 & 0 \end{bmatrix}_{3n\times n} \\ \boldsymbol{G}_{pq}=\begin{bmatrix} \langle S_{a(1)}\rangle_{p-q}^E & \langle S_{a(2)}\rangle_{p-q}^E & 0 \end{bmatrix}^{\mathrm{T}} \quad p,q\in\{1,2,\ldots,n\} \end{cases} \tag{14}$$

$$\begin{cases} \boldsymbol{A}_{21}=-\dfrac{3}{C}\begin{bmatrix} H_{11} & H_{12} & \cdots & H_{1n} \\ H_{21} & H_{22} & \cdots & H_{12} \\ \vdots & \vdots & & \vdots \\ H_{n1} & H_{n2} & \cdots & H_{nn} \end{bmatrix} \\ \boldsymbol{H}_{pq}=\begin{bmatrix} \langle S_{a(2)}\rangle_{p-q}^E & \langle S_{a(1)}\rangle_{p-q}^E & 0 \end{bmatrix}^{\mathrm{T}} \quad p,q\in\{1,2,\ldots,n\} \end{cases} \tag{15}$$

$$\boldsymbol{A}_{22}=\mathrm{diag}\left(0,-\mathrm{j}\omega,-\mathrm{j}2\omega,\ldots,-\mathrm{j}(n-3)\omega,-\mathrm{j}(n-2)\omega,-\mathrm{j}(n-1)\omega\right) \tag{16}$$

where * represents the conjugate operator. $\boldsymbol{A}_{12}$ and $\boldsymbol{A}_{21}$ are composed of the EDPSCs of the switching functions. Because of the three-phase three-wire connection of the inverter shown in Fig. 1, there are no zero-sequence components in the currents at the AC side. The elements of corresponding columns and rows are zero.

Among these coefficient matrices, $\boldsymbol{A}_{11}$ and $\boldsymbol{A}_{22}$ are diagonal matrices. Therefore, the EDPSCs of the current at the AC side and the EDPs of voltage at the DC side are decoupled. $\boldsymbol{A}_{12}$ and $\boldsymbol{A}_{21}$ represent the interactions between the current interharmonics at the AC side and voltage interharmonics at the DC side, which can describe the generation principles and interactions among interharmonics.

Equation (12) can be simplified as:

$$\frac{\mathrm{d}\boldsymbol{X}}{\mathrm{d}t}=\boldsymbol{A}\boldsymbol{X}+\boldsymbol{U} \tag{17}$$

where $\boldsymbol{X}=\begin{bmatrix}\boldsymbol{X}_1\\ \boldsymbol{X}_2\end{bmatrix}$; $\boldsymbol{A}=\begin{bmatrix}\boldsymbol{A}_{11} & \boldsymbol{A}_{12}\\ \boldsymbol{A}_{21} & \boldsymbol{A}_{21}\end{bmatrix}$; $\boldsymbol{U}=\begin{bmatrix}-\boldsymbol{U}_1/L\\ \boldsymbol{U}_2/C\end{bmatrix}$.

Equation (17) is referred to as the interharmonic analysis model of the PVGS.

C. Generation Principles and Interactions

The generation principles and interactions among interharmonics can be attained by solving the proposed interharmonic analysis model, as shown in (17).

For example, the interharmonics near the power frequency are analyzed using the model. The relationship between the power angular frequency and the selected fundamental angular frequency is $\omega_s=m\omega$. According to [25], if the standard sinusoidal pulse width modulation (PWM) is applied, most of the EDPSCs of the switching function are zero, whereas the positive-sequence components of the power frequency are the modulation ratio, which is $\langle S_{a(1)}\rangle_m^E=M$ and M is the modulation ratio. As a consequence, there are only three equations for the k^{th} voltage interharmonic at the DC side in (12), as shown in (18). Interharmonic interactions can be decoupled with the EDPSCs.

$$\begin{cases} \dfrac{\mathrm{d}\langle I_{a(1)}\rangle_{k+m}^E}{\mathrm{d}t}=\dfrac{-R-\mathrm{j}(k+m)\omega L}{L}\langle I_{a(1)}\rangle_{k+m}^E-\dfrac{1}{L}\langle U_{sa(1)}\rangle_{k+m}^E+\dfrac{1}{L}\langle S_{a(1)}\rangle_m^E\langle U_{dc}\rangle_k^E \\ \dfrac{\mathrm{d}\langle I_{a(2)}\rangle_{k-m}^E}{\mathrm{d}t}=\dfrac{-R-\mathrm{j}(k-m)\omega L}{L}\langle I_{a(2)}\rangle_{k-m}^E-\dfrac{1}{L}\langle U_{sa(2)}\rangle_{k-m}^E+\dfrac{1}{L}\langle S_{a(1)}\rangle_m^{E^*}\langle U_{dc}\rangle_k^E \\ \dfrac{\mathrm{d}\langle U_{dc}\rangle_k^E}{\mathrm{d}t}=-3\dfrac{1}{C}\left(\langle S_{a(1)}\rangle_m^{E^*}\langle I_{a(1)}\rangle_{k+m}^E+\langle S_{a(1)}\rangle_m^E\langle I_{a(2)}\rangle_{k-m}^E\right)+\dfrac{1}{C}\langle I_{pv}\rangle_k^E-\mathrm{j}k\omega\langle U_{dc}\rangle_k^E \end{cases} \tag{18}$$

By solving (18), the generation principles and interactions among interharmonics can be described mathematically. For steady-state analysis, the differential terms at the left side are set to be 0, and the differential equations are simplified as algebraic equations, as shown in (19).

$$\begin{cases} \langle I_{a(1)}\rangle_{k+m}^E=\dfrac{\langle S_{a(1)}\rangle_m^E\langle U_{dc}\rangle_k^E-\langle U_{sa(1)}\rangle_{k+m}^E}{R+\mathrm{j}(k+m)\omega L} \\ \langle I_{a(2)}\rangle_{k-m}^E=\dfrac{\langle S_{a(1)}\rangle_m^{E^*}\langle U_{dc}\rangle_k^E-\langle U_{sa(2)}\rangle_{k-m}^E}{R+\mathrm{j}(k-m)\omega L} \\ \langle U_{dc}\rangle_k^E=\dfrac{-3\left(\langle S_{a(1)}\rangle_m^{E^*}\langle I_{a(1)}\rangle_{k+m}^E+\langle S_{a(1)}\rangle_m^E\langle I_{a(2)}\rangle_{k-m}^E\right)}{\mathrm{j}k\omega C}+\dfrac{\langle I_{pv}\rangle_k^E}{\mathrm{j}k\omega C} \end{cases} \tag{19}$$

Equation (19) can be presented as an equivalent circuit as shown in Fig. 2. Based on Fig. 2, the generation principles and interactions among interharmonics are given as follows.

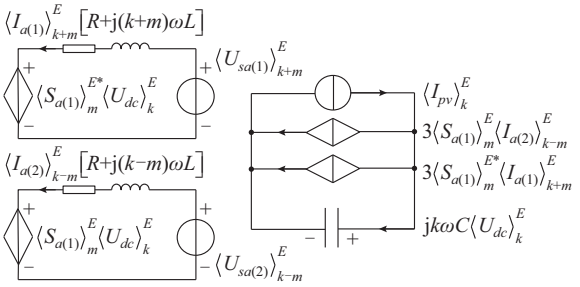

Fig. 2. Equivalent circuit of generation and interaction characteristics of interharmonics in PVGS.

1) If the fluctuating outputs of the PV have a low frequency f, a voltage interharmonic with f will be generated at the DC side, and two current interharmonics with frequency $f_s\pm f$ will be generated further at the AC side, where f_s is the power frequency. The lower the interharmonic frequency, the lower the impendence at the AC side and the larger the amplitude of the current interharmonics.

2) If the AC system source contains a positive-sequence voltage interharmonic with f, a current interharmonic with

the same frequency will be generated at the AC side. With the interactions, a voltage interharmonic with frequency $|f_s - f|$ is generated at the DC side. The current interharmonic with the frequency $|2f_s - f|$ will be generated at the AC side.

3) If the AC system source contains a negative-sequence voltage interharmonic with f, a current interharmonic with the same frequency will be generated at the AC side. With the interactions, a voltage interharmonic with frequency $f_s + f$ is generated at the DC side. A current interharmonic with frequency $2f_s + f$ will further be generated at the AC side.

IV. Simulation and Experimental Test

A. Simulation Test

A simulation model of the PVGS is established using MATLAB/Simulink, as shown in Fig. 3. In the simulation model, the nominal source voltage of AC system is 380 V. The resistance and reactance at the AC side are 0.02 Ω and 5 mH, respectively. The capacitor at the DC side is 3400 μF. The rated power of the PV array is 56 kW. The PWM is naturally the sampling modulation. The modulation signal frequency is 50 Hz, and the carrier signal frequency is 7.5 kHz.

The interharmonics around the power frequency are addressed. The fundamental frequency of the EDPs and EDPSCs is selected as 5 Hz.

To verify the generation principles and interactions among interharmonics obtained in Section III, three scenarios are considered. Scenario 1 is the PV output with fluctuation; scenario 2 is the the source voltage of AC system with positive-sequence voltage distortion; and scenario 3 is the the source voltage of AC system with negative-sequence voltage distortion. In scenario 1, it is supposed that the PV exhibits fluctuating outputs with the two different frequency components, which are 5 Hz and 25 Hz, by changing the illumination intensity in the simulation model. The source voltage of AC system is ideal. The PV output current contains 5 Hz and 25 Hz fluctuations. The amplitude of the fluctuations is 2%-10% of the nominal voltage.

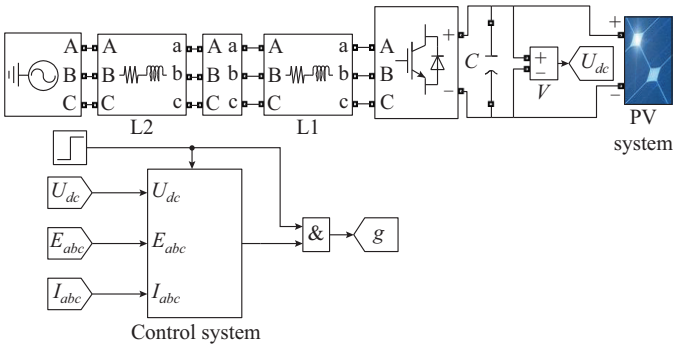

Fig. 3. Simulation model of PVGS.

The comparisons of the calculation and simulation results of the voltage at the DC side and the current of phase a are presented in Table I. The calculation results are very close to the simulation results. Because of the fluctuation of the PV output current, voltage interharmonics with frequencies of 5 Hz and 25 Hz are observed at the DC side. Simultaneously, the corresponding interharmonic currents with frequencies of 50 ± 5 Hz and 50 ± 25 Hz are generated at the AC side because of the interactions between the AC and DC sides. The amplitude of the current interharmonics with a frequency of 50 ± 25 Hz is smaller than that with a frequency of 50 ± 5 Hz, which verifies the first principle.

TABLE I
Comparison of Simulation and Calculation Results (Scenario 1)

Harmonic ratio (%)	U_{dc}						I_a									
	Simulation			Calculation			Simulation					Calculation				
	0 Hz	5 Hz	25 Hz	0 Hz	5 Hz	25 Hz	25 Hz	45 Hz	50 Hz	55 Hz	75 Hz	25 Hz	45 Hz	50 Hz	55 Hz	75 Hz
2	740	0.228	0.861	740.101	0.228	0.861	1.284	1.194	118.193	1.194	1.289	1.285	1.194	118.219	1.194	1.289
4	740	0.456	1.722	740.096	0.457	1.722	2.569	2.388	118.197	2.388	2.578	2.570	2.388	118.221	2.388	2.579
6	740	0.685	2.586	740.106	0.686	2.586	3.853	3.581	118.201	3.582	3.870	3.854	3.581	118.227	3.583	3.871
8	740	0.914	3.452	740.147	0.916	3.451	5.136	4.773	118.209	4.777	5.163	5.138	4.774	118.241	4.778	5.164
10	740	1.144	4.319	740.080	1.146	4.319	6.418	5.966	118.218	5.972	6.457	6.420	5.966	118.240	5.973	6.458

The spectra of the voltage at the DC side and the current of phase a are shown in Fig. 4. As the amplitude of the disturbances increases, the amplitude of the interharmonics increases, whose frequency is different from that of interharmonics as shown in the principles in Section III. These interharmonics are introduced by the switching functions affected by the interharmonics as shown in the principles. In fact, when the amplitude of the disturbances is small, only the fundamental components of the switching functions should be considered in the interharmonic analysis (corresponding to (19)). When the amplitude of disturbances is large, other switching function components introduced by the interharmonics as shown in the principles should be considered (corresponding to (17)).

In scenario 2, a positive-sequence voltage distortion with a 45 Hz interharmonic is overlaid in the source voltage of AC system. The amplitude of the distortion voltage is within 2%-10% of the nominal voltage. The comparisons of the calculation and simulation results are listed in Table II.

A current interharmonic is observed in phase a with a frequency of 45 Hz because of the background voltage distortion. Simultaneously, a voltage interharmonic with a frequency of 5 Hz appears in the voltage at the DC side because of the interactions between the AC and DC sides. A current interharmonic is observed in phase a with a frequency of 55 Hz because of the interactions, which verifies the second principle.

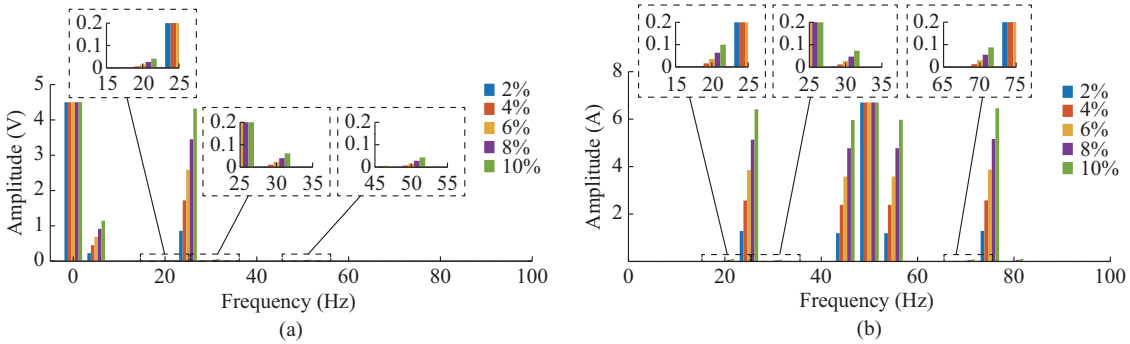

Fig. 4. Simulation results of PV output fluctuates. (a) Spectrum of voltage at DC side. (b) Spectrum of current of phase a.

TABLE II
COMPARISON OF SIMULATION AND CALCULATION RESULTS (SCENARIO 2)

Harmonic ratio (%)	U_{dc}				I_a					
	Simulation		Calculation		Simulation			Calculation		
	0 Hz	5 Hz	0 Hz	5 Hz	45 Hz	50 Hz	55 Hz	45 Hz	50 Hz	55 Hz
2	740	0.210	740.675	0.209	0.187	118.189	2.497	0.184	118.306	2.499
4	740	0.419	740.639	0.417	0.372	118.181	4.994	0.367	118.292	4.998
6	740	0.627	740.636	0.625	0.557	118.167	7.489	0.548	118.277	7.495
8	740	0.835	740.657	0.832	0.740	118.147	9.983	0.729	118.261	9.991
10	740	1.044	740.589	1.039	0.923	118.122	12.475	0.911	118.225	12.484

In scenario 3, a negative-sequence voltage distortion with 5 Hz interharmonic is overlaid in the source voltage of AC system. The amplitude of the distortion voltage is 2%-10% of the nominal voltage. The comparisons of the calculation and simulation results are given in Table III. There is also a current interharmonic in phase a with a frequency of 5 Hz since the background voltage distortion is also observed. Simultaneously, a voltage interharmonic with a frequency of 55 Hz appears in the voltage at the DC side owing to the interactions between the AC and DC sides. There is a current interharmonic in phase a with a frequency of 105 Hz, owing to the interactions, which verifies the third principle.

TABLE III
COMPARISON OF SIMULATION AND CALCULATION RESULTS (SCENARIO 3)

Harmonic ratio (%)	U_{dc}				I_a					
	Simulation		Calculation		Simulation			Calculation		
	0 Hz	55 Hz	0 Hz	55 Hz	5 Hz	50 Hz	105 Hz	5 Hz	50 Hz	105 Hz
2	740	0.589	740.688	0.604	0.649	118.199	0.825	0.643	118.215	0.826
4	740	1.177	740.687	1.189	1.299	118.221	1.647	1.299	118.232	1.648
6	740	1.766	740.612	1.775	1.949	118.258	2.460	1.952	118.266	2.461
8	740	2.355	740.646	2.362	2.600	118.310	3.266	2.611	118.318	3.267
10	740	2.944	740.634	2.952	3.251	118.377	4.068	3.268	118.385	4.070

The simulation results of source voltage of AC system with positive-sequence voltage distortion and negative-sequence voltage distortion are presented in Figs. 5 and 6, respectively. As the amplitude of disturbances increases, the amplitude of the interharmonics increases, whose frequency is different from that shown in the principles in Section III. This phenomenon is similar to the one in scenario 1, and the same conclusions can be drawn.

B. Experimental Test

An experimental platform has been established to verify the presented model and the principles attained. The PV arrays are simulated using a programmable DC power supply. The controllers of the PV inverter and the programmable DC power supply are designed based on a digital signal processor (DSP) TMS320F28335. The inverter is applied with the intelligent power module (IPM) PM150RL1A120. The resistance and reactance at the AC side are 0.02 Ω and 5 mH, respectively. The capacitor at the DC side is 3400 μF.

An isolated transformer is set up between the inverter and the power grid. The remaining parameters are consistent with the simulation model. The voltage at the DC side and the current of phase a are monitored by two digital oscilloscopes, DSO-X 3024A, whose sampling frequency is 40.96 kHz and the measurement accuracy reaches level A in IEC61000-4-7 [25].

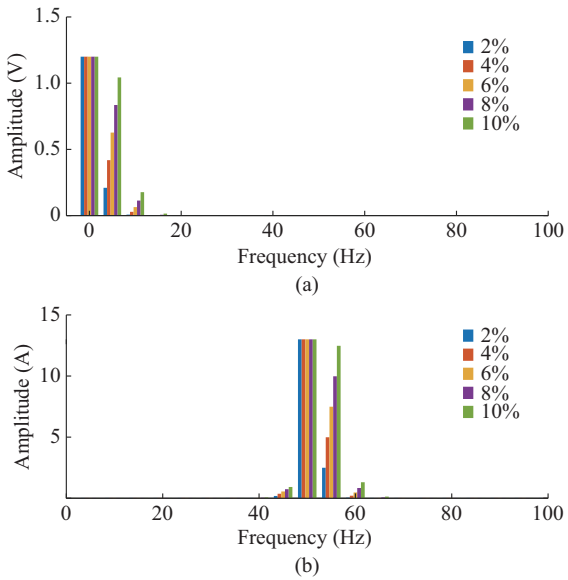

Fig. 5. Simulation results of source voltage of AC system with positive-sequence voltage distortion. (a) Spectrum of voltage at DC side. (b) Spectrum of current of phase a.

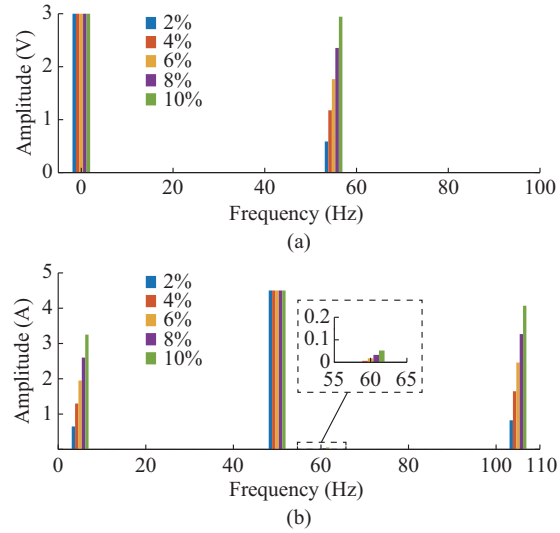

Fig. 6. Simulation results of source voltage of AC system with negative-sequence voltage distortion. (a) Spectrum of voltage at DC side. (b) Spectrum of current of phase a.

The fluctuating currents with different frequencies and amplitudes are injected into the DC side by adjusting the outputs of the programmable DC power supply to simulate the fluctuating outputs of the PV arrays. The frequency and amplitude of the injected currents are measured, and the results are listed in Table IV. The waveforms and spectrums of the current of phase a and the voltage at the DC side are recorded by digital oscilloscopes, which are shown in Supplement A Figs. SA1 and SA2. As shown in the experimental results, when there are 5 Hz (or 75 Hz) DC current fluctuations injected into the DC side, the voltage interharmonics with the same frequency appear at the DC side. There are also 50 ± 5 Hz (or 75 ± 50 Hz) current interharmonics generated at the AC side. Thus, the first principle is verified. Since the AC system source voltage cannot be controlled in this experimental platform, the other two principles have not been tested experimentally. By solving (12) with the given parameters, the voltage interharmonics at the DC side and the current interharmonics at the AC side can be calculated. The experimental results are compared with the calculation results in Table V. The calculation results are very close to the experimental results, which verifies the correctness of the presented model.

TABLE IV
FREQUENCY AND AMPLITUDE OF DC DISTURBING CURRENT OF INVERTER

Frequency of disturbance f_h (Hz)	Amplitude of disturbance I_h (A)
5	0.307
75	0.776

TABLE V
COMPARISON OF EXPERIMENTAL AND CALCULATION RESULTS

Type	Frequency (Hz)	Value (V)	
		Experiment	Calculation
Interharmonic voltage at DC side	5	3.890	3.872
	75	0.634	0.606
Interharmonic current of phase a at AC side	25	0.487	0.506
	45	0.170	0.174
	55	0.115	0.116
	125	0.451	0.481

V. CONCLUSION

In this paper, DPs and DPSCs are extended into the EDPs and EDPSCs in granularity with consistent characteristics by selecting one suitable fundamental frequency. With the decoupling characteristics of the EDPSCs, the interaction principles are described clearly. The generation principles and interactions among interharmonics in the PVGS are presented. By comparing the calculation, simulation, and experimental results, the presented model and principles are proven to be useful for the analysis of the interharmonics in the PVGS.

By changing the fundamental frequency, the presented model can be used to analyze the interharmonics with different frequencies in detail. For the interharmonics with different amplitudes, most of the EDPSCs of the switching function are zero when the fluctuating power outputs from PVs at the DC side and background voltage distortions at the AC side are small. Equation (19) is useful for analyzing the interharmonics. Otherwise, (17) has to be applied, which increases the space complexity but ensures the calculation accuracy of the interharmonics.

REFERENCES

[1] J. Sun, M. Li, Z. Zhang *et al.*, "Renewable energy transmission by HVDC across the continent: system challenges and opportunities," *CSEE Journal of Power and Energy Systems*, vol. 3, no. 4, pp. 353-364, Dec. 2017.
[2] A. Ahmed and T. Jiang, "Operation management of power grid system with renewable energy sources and energy storage system integrations," in *Proceedings of 2018 2nd IEEE Conference on Energy Internet and Energy System Integration (EI2)*, Beijing, China, Oct. 2018, pp. 1-6.
[3] X. Liang, "Emerging power quality challenges due to integration of re-

newable energy sources," in *Proceedings of 2016 IEEE Industry Applications Society Annual Meeting*, Portland, USA, Oct. 2016, pp. 1-9.
[4] A. Testa, M. F. Akram, R. Burch *et al*., "Interharmonics: theory and modeling," *IEEE Transactions on Power Delivery*, vol. 22, no. 4, pp. 2335-2348, Oct. 2007.
[5] R. K. Varma, S. A. Rahman, T. Vanderheide *et al*., "Harmonic impact of a 20-MW PV solar farm on a utility distribution network," *IEEE Power and Energy Technology Systems Journal*, vol. 3, no. 3, pp. 89-98, Sept. 2016.
[6] R. Yacamini, "Power system harmonics, IV: interharmonics," *Power Engineering Journal*, vol. 10, no. 4, pp. 185-193, Aug. 1996.
[7] E. W. Gunther, "Interharmonics in power systems," in *Proceedings of 2001 IEEE PES Summer Meeting*, Vancouver, Canada, Jul. 2001, pp. 813-817.
[8] L. Chen, W. Zhao, and F. Wang, "An interharmonic phasor and frequency estimator for subsynchronous oscillation identification and monitoring," *IEEE Transactions on Instrumentation and Measurement*, vol. 68, no. 6, pp. 1714-1723, Jun. 2019.
[9] A. Luo, N. Xie, Z. Shuai *et al*., "Large-scale photovoltaic plant harmonic transmission model and analysis on resonance characteristic," *IET Power Electronics*, vol. 8, no. 4, pp. 565-573, Apr. 2015.
[10] P. Poovarasan and P. Saraswathi, "Implementation of MLI and THD analysis for grid connected PV system and simulation study of voltage stability with change in grid impedance," in *Proceedings of 2015 International Conference on Circuits, Power and Computing Technologies (ICCPCT)*, Nagercoil, India, Mar. 2015, pp. 1-6.
[11] J. B. Kwon, X. Wang, F. Blaabjerg *et al*., "Harmonic instability analysis of a single-phase grid-connected converter using a harmonic state-space modeling method," *IEEE Transactions on Industry Applications*, vol. 52, no. 5, pp. 4188-4200, Sept. 2016.
[12] P. Liu, M. Deng, J. Wang *et al*., "Analysis about the parameters calculation of characteristic interharmonic in the voltage source type AC/DC/AC frequency converter," in *Proceedings of China International Conference on Electricity Distribution (CICED)*, Shanghai, China, Sept. 2012, pp. 1-5.
[13] D. J. Hume, A. R. Wood, and C. M. Osauskas, "Frequency-domain modelling of interharmonics in HVDC systems," *IEE Proceeding: Generation, Transmission and Distribution*, vol. 150, no. 1, pp. 41-48, Jan. 2003.
[14] S. Djurovic, D. S. Vilchis-Rodrigue, and A. C. Smith, "Supply induced interharmonic effects in wound rotor and doubly-fed induction generators," *IEEE Transactions on Energy Conversion*, vol. 30, no. 4. pp. 1397-1408, Dec. 2015.
[15] P. Gnacinski and M. Peplinski, "Induction cage machine supplied with voltage containing subharmonics and interharmonics," *IET Electronic Power Application*, vol. 8, no. 8, pp. 287-295, Sept. 2014.
[16] T. Messo, A. Jokipii, A. Aapro *et al*., "Time and frequency-domain evidence on power quality issues caused by grid-connected three-phase photovoltaic inverters," in *Proceedings of 16th European Conference on Power Electronics and Applications*, Lappeenranta, Finland, Aug. 2014, pp. 1-9.
[17] Y. Pan, A. Sangwongwanich, Y. Yang *et al*., "A phase-shifting MPPT to mitigate interharmonics from cascaded H-bridge PV inverters," *IEEE Transactions on Industry Applications*, doi: 10.1109/TIA.2020.3000969
[18] A. Sangwongwanich, Y. Yang, D. Sera *et al*., "Analysis and modeling of interharmonics from grid-connected photovoltaic systems," *IEEE Transactions on Power Electronics*, vol. 33, no. 10, pp. 8353-8364, Oct. 2018.
[19] L. Feola, R. Langella, P. Marino *et al*., "On the effects of interharmonic distortion on grid connected three-phase PV inverter," in *Proceedings of IEEE 15th International Conference on Harmonics and Quality of Power*, Hong Kong, China, Jun. 2012, pp. 682-688.
[20] C. Hou, M. Zhu, Z. Li *et al.*, "Inter harmonic THD amplification of voltage source converter: concept and case study," *IEEE Transactions on Power Electronics*, vol. 35, no. 12, pp. 12651-12656, Dec. 2020.
[21] Q. Zhong, L. Lin, and G. Wang, "Harmonic analysis model for voltage source converter under unbalanced conditions," *IET Generation, Transmission & Distribution*, vol. 9, no. 1, pp. 12-21, Jan. 2015.
[22] G. Frigo, G. Giorgi, and C. Narduzzi, "Efficient detection for multifrequency dynamic phasor analysis," in *Proceedings of 7th IEEE International Workshop on Applied Measurements for Power Systems (AMPS)*, Aachen, Germany, Sept. 2016, pp. 28-30.
[23] J. A. de la O. Serna, "Dynamic phasor estimates for power system oscillations," *IEEE Transactions on Instrumentation and Measurement*, vol. 56, no. 5, pp. 1648-1657, Oct. 2007.
[24] R. Langella, A. Testa, and A. E. Emanuel, "Unbalance definition for electrical power systems in the presence of harmonics and interharmonics," *IEEE Transactions on Instrumentation and Measurement*, vol. 61, no. 10, pp. 2622-2631, Oct. 2012.
[25] *Electromagnetic Compatibility (EMC)-Part 4-7: Testing and Measurement Techniques-General Guide on Harmonics and Interharmonics Measurements and Instrumentation, for Power Supply Systems and Equipment Connected Thereto*, IEC Standard 61000, 2009.

Qing Zhong received the B.Sc. degree in North China University of Technology, Beijing, China, in 1997, and the MS.c. and Ph.D. degrees in South China University of Technology, Guangzhou, China, in 2003 and 2000, respectively, all in electrical engineering. He is now a Professor in the School of Electric Power, South China University of Technology. His research interests include power quality and power electronics control.

Yangxin Qiu received the B.Sc. degree in South China University of Technology, Guangzhou, China, in 2017. He is now a Ph.D. student in School of Electric Power, South China University of Technology. His research interests include power quality and power electronics control.

Yuming Zhao received the B.Sc. and Ph.D. degrees in Tsinghua University, Beijing, China, in 2006 and 2010, respectively, all in electrical engineering. He is now a Senior Engineer of Professor level in Shenzhen Power Supply Company, Shenzhen, China. His research interests include HVDC and low-voltage DC system analysis, control and protection.

Haifeng Li received the Ph.D. degree in electrical engineering in South China University of Technology, Guangzhou, China, in 2004. He is currently an Associate Professor in the School of Electric Power Engineering, South China University of Technology. His research interests include power system protection and control, smart distribution networks, and HVDC technology.

Gang Wang is now the Professor in School of Electric, South China University of Technology, Guangzhou, China. His research interests include power system relaying, automation and control.

Fushuan Wen received the B.E. and M.E. degrees from Tianjin University, Tianjin, China, in 1985 and 1988, respectively, and the Ph.D. degree from Zhejiang University, Hangzhou, China, in 1991, all in electrical engineering. He joined the faculty of Zhejiang University in 1991, and has been a Full Professor since 1997. He is also a part-time Distinguished Professor under Yusheng XUE Education Foundation in Hangzhou Dianzi University, Hangzhou, China. He had been a university Distinguished Professor, the Deputy Dean of the School of Electrical Engineering and the Director of the Institute of Power Economics and Electricity Markets in South China University of Technology, Guangzhou, China, from 2005 to 2009. He is the Editor-in-Chief of IET Energy Conversion and Economics, and a Deputy Editor-in-Chief of Automation of Electric Power Systems. His research interests include power industry restructuring, power system alarm processing, fault diagnosis and restoration strategies, as well as smart grid and electric vehicle.